LASER & PHOTONICS REVIEWS
www.lpr-journal.org

Adaptive Optics-Assisted Long-Term 3D Fluorescence and Intensity Diffraction Tomography for High Spatiotemporal Resolution Cellular Imaging

Ning Zhou, Runnan Zhang, Ruizhi Zhu, Zihao Zhou, Hongjun Wu, Qian Chen, Peng Gao, Jiasong Sun,* and Chao Zuo**

Intensity diffraction tomography (IDT) and fluorescence dual-modality imaging facilitate a comprehensive analysis of biological components and their interactions. However, long-term imaging is typically compromised by environmental thermal fluctuations and mechanical disturbances from the microscope, leading to time-varying aberrations and focus drift that degrades the performance of long-term imaging and the accuracy of dual-modality colocalization. To counter these issues, an adaptive optics-assisted 3D dual-modality imaging method (AO-FIDT) is developed. The method utilizes an innovative iterative ptychographic approach, paired with annular matched illumination conditions, to precisely reconstruct IDT results and characterize the aberrations in real-time. Furthermore, feedback on the real-time aberrations to the point spread function of the system is provided to synchronously correct the 3D fluorescence results. The efficacy and precision of AO-FIDT are confirmed through long-term, high-resolution imaging of HeLa cells. Furthermore, by scrutinizing the morphological characteristics of subcellular organelles in live COS-7 cells, including progressive sphericity in mitochondria under phototoxicity, and by monitoring the continuous changes in mitochondrial dynamics throughout the cell division process, the broad applicability of AO-FIDT in analyzing subcellular organelle structure and function is demonstrated.

1. Introduction

Microscopes offer a unique and powerful method to observe cells and molecules across time and space. However, visualizing cellular structures is challenging since biological samples are mostly water and have poor refractive properties.[1] 3D fluorescence microscopy, which obtains molecular-specific information by labeling specific molecules within cells with fluorescent proteins or dyes and characterizes living cells and their 3D subcellular structures using axial scanning[2] or focal sweeping[3] technologies, provides researchers with a valuable tool for biomedical research and clinical applications.[4] However, fluorescence labeling has its limitations. First, fluorescence microscopy sacrifices the overall view of interacting partners and the surrounding environment to achieve high contrast, thus failing to provide a comprehensive view of the cellular landscape.[5] Additionally, substantial phototoxicity and photobleaching pose significant challenges to the sample, necessitating a trade-off between the quality of data and the timescale of live-cell imaging.[6] These factors constrain the application of fluorescence microscopy in long-term experiments on living cells.

Optical diffraction tomography (ODT) is an emerging 3D microscopy technique that leverages the intrinsic refractive index (RI) of transparent biological samples as a natural contrast mechanism, enabling label-free imaging.[7,8] Compared to fluorescence microscopy, ODT technology effectively avoids the phototoxicity and photobleaching issues that may arise from fluorescent dyes, giving it a unique advantage in the long-term observation of living cells.[9,10] It should be noted that while the measured 3D-RI distribution provides label-free analysis of cells and subcellular organelles, it has certain limitations in obtaining molecular-specific information. For instance, most proteins have similar RI increments, making distinguishing specific proteins within each cellular component difficult based on the measured RI distribution.[11]

In response to the challenges mentioned above, a dual-modality imaging approach that combines fluorescence imaging

N. Zhou, R. Zhang, R. Zhu, Z. Zhou, H. Wu, J. Sun, C. Zuo
Smart Computational Imaging Laboratory (SCILab)
School of Electronic and Optical Engineering
Nanjing University of Science and Technology
Nanjing, Jiangsu 210094, China
E-mail: sunjiasong@njust.edu.cn; zuochao@njust.edu.cn

N. Zhou, R. Zhang, R. Zhu, Z. Zhou, H. Wu, Q. Chen, J. Sun, C. Zuo
Jiangsu Key Laboratory of Spectral Imaging & Intelligent Sense
Nanjing University of Science and Technology
Nanjing, Jiangsu 210094, China

N. Zhou, R. Zhang, R. Zhu, Z. Zhou, H. Wu, Q. Chen, J. Sun, C. Zuo
Smart Computational Imaging Research Institute (SCIRI) of Nanjing University of Science and Technology
Nanjing, Jiangsu 210094, China

P. Gao
School of Physics
Xidian University
Xi'an 710126, China
E-mail: peng.gao@xidian.edu.cn

The ORCID identification number(s) for the author(s) of this article can be found under https://doi.org/10.1002/lpor.202402196

DOI: 10.1002/lpor.202402196

and ODT has emerged,[12,13] providing a novel solution for the 3D observation of living cells. However, existing ODT schemes in dual-modality imaging are based on interference schemes, which are difficult to reconcile with commercial microscopes, thereby limiting the universality of the technology. On the other hand, long-term (from hours to days) 3D imaging still faces a fundamental challenge: the optical heterogeneity of cells, environmental thermal fluctuations, and the mechanical instability of the microscope structure can all potentially contribute to time-varying aberrations and focus drift. It should be noted that in the field of 3D optical microscopy, the traditional distinction between the focal plane and defocused planes has become blurred. Despite defocus, critical information can still be captured in other layers. However, focus drifts significantly interfere with the long-term tracking and observation of subcellular organelles and pose a challenge to precise axial colocalization in dual-modality imaging.[14,15] Furthermore, higher-order aberrations other than defocus are sample- and environment-dependent, cannot be compensated by a fixed optical design, and require fast dynamic correction during imaging. Therefore, achieving aberration correction in 3D dual-modality imaging to obtain long-term, high spatiotemporal resolution dynamic 3D reconstruction results remains a significant issue in the field.

To ensure stable, high-quality imaging results over extended observation periods, researchers have employed various methods to compensate for time-varying aberrations. Komatsu et al.[16] utilized the z-axis drift compensator of the microscope to ensure that images remained focused throughout continuous multi-day observations, supporting high-precision and rapid cell analysis. However, mechanical compensation can only remove out-of-focus aberrations. Recently, a technique known as computational adaptive optics (AO) has been developed to address the time-varying aberrations of the imaging system by algorithmically correcting,[17–19] eliminating the need for additional hardware compensation. Based on this concept, Shu et al.[20] have leveraged the inherent data redundancy in Fourier ptychographic microscopy (FPM) to recover directly and correct aberrations using AO, achieving high-quality long-term quantitative phase imaging (QPI) results. Similarly, Lu et al.[21] have also achieved long-term high-throughput QPI measurements by eliminating spatially non-uniform and time-varying aberrations through aberration-corrected intensity transmission QPI. However, these methods are all applied in 2D QPI imaging. To our knowledge, the application of adaptive optics-assist technology to address time-varying aberrations in 3D dual-modality imaging has not been reported.

In this work, we propose an adaptive optics-assisted, non-interferometric 3D fluorescence and intensity diffraction tomography dual-modality imaging method, termed AO-FIDT, for long-term high spatiotemporal resolution cellular imaging. Based on the Fourier ptychographic framework,[22–24] we uniquely introduce AO-assisted in the intensity diffraction tomography (IDT) module and derive the time-varying aberration update model of the imaging system, enabling the separation of the coupled 3D refractive index (RI) and aberrations from the captured unlabeled intensity images. Concurrently, the fluorescence module feeds back the real-time calculated aberration solution into the point spread function (PSF) of the system and combines it with the 3D Richardson-Lucy (RL) algorithm[25,26] to obtain the 3D fluorescence results after AO-assisted correction. Combining an annular numerical aperture (NA) matched illumination configuration,[27,28] the IDT module achieved achieves a half-width resolution of 175 nm laterally and 775 nm axially at a volume imaging speed of 7.5 Hz ($160 \times 160 \times 30\ \mu m^3$). The fluorescence module acquires the image stacks using axial scanning, and the result is used to guide the interpretation of the observed structures in the IDT module. By imaging the 3D RI of live HeLa cells and the long-term dual-modality imaging of live COS-7 cells, we have demonstrated the unique advantages of AO-FIDT in imaging cells, structures, and processes that are susceptible to phototoxicity, such as cell mitosis. Theoretical evaluations and experimental results indicate that AO-FIDT has the potential to become a valuable 3D imaging tool for exploring the relationship between the biophysical/biochemical properties of cells and their molecular characteristics/processes.

2. Principles and Methods

Figure 1a illustrates the main steps of the 3D RI reconstruction and imaging system aberration correction workflow. Using a simulated 3D cell as an example, the following steps are: First, the LED sequentially illuminates the sample to capture intensity images under illumination angle scanning. Then, the captured intensity images are used to apply intensity constraints in a single instance to update the 3D scattering potential and pupil function jointly. Here, the pupil function is characterized by Zernike polynomials to achieve efficient and accurate correction. In conjunction with the fast-adaptive relaxation technique we introduced earlier,[29] we perform iterative constraints continuously until the outcomes converge to the intensity images that have been captured. The recovered 3D scattering potential spectrum and the aperture function containing time-varying aberrations can then be obtained in K-space, as shown in the second column of Figure 1a. Section S1 (Supporting Information), details the comprehensive iterative process. Owing to the constraints on projection angles set by the NA of a single objective lens, it is not possible to measure the spatial frequency components along the axial dimension.[30] Therefore, we use an iterative, non-negative constraint-based post-processing algorithm[31] to computationally fill in this missing information. Finally, a 3D inverse Fourier transform is utilized on the scattering potential spectrum in order to reconstruct the 3D RI distribution of the sample.

For the 3D fluorescence imaging part, we simulated the process of fluorescence imaging of cellular lipid droplets. First, the original intensity image stack of wide-field fluorescence is collected through axial scanning, as shown in Figure 1b. Axial scanning can gather all 3D information about the sample. However, it should be noted that to reduce phototoxicity and photobleaching and to avoid motion blur, we typically choose a shorter exposure time. This causes the captured images to be affected by Poisson noise, and the quality decreases. At the same time, deconvolution methods tend to amplify noise, so regularization constraints based on image priors are necessary to reduce noise sensitivity. Here, we combined a 3D iterative RL algorithm,[32–34] which calculates the maximum likelihood estimate adapted to Poisson statistics, and a total variation (RL-TV) based regularization constraint to suppress unstable oscillations while preserving object edges. It should be noted that we feed back the calculated aberration solution obtained from the IDT module into the PSF of

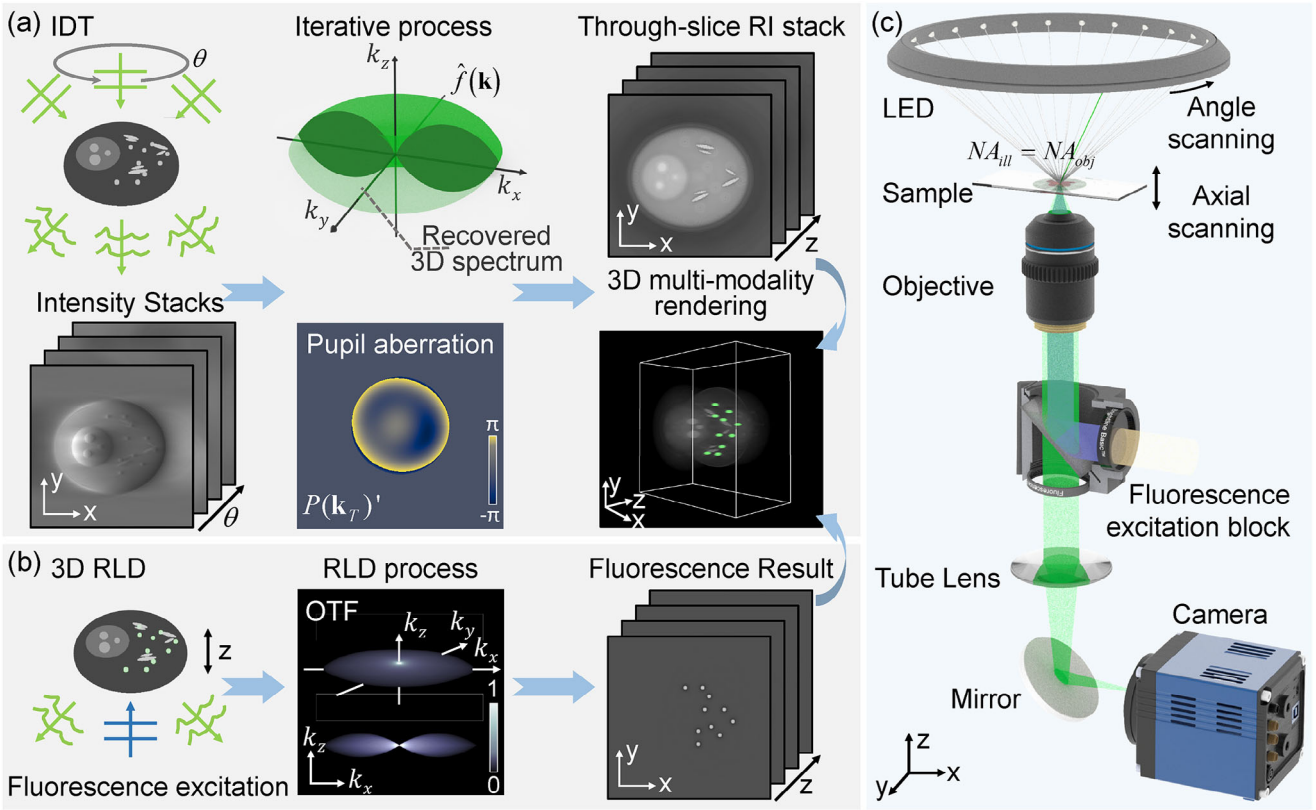

Figure 1. Experimental implementation and image reconstruction of AO-FIDT. a) Main steps of the AO-IDT flowchart for 3D RI reconstruction of simulated cell phantom. b) Flowchart of the 3DRL deconvolution algorithm for solving 3D fluorescence results. c) System schematic diagram.

the system and then bring the updated PSF into the 3D RL algorithm to get the 3D fluorescence result, which eliminates the time-varying aberration. The detailed process of the AO-assisted 3D RL algorithm is presented in Section S2 (Supporting Information).

To achieve long-term, high spatiotemporal resolution dual-modality imaging of cells, we constructed the AO-FIDT system, as shown in Figure 1c. The device takes advantage of non-interferometric measurement and can be directly integrated with a commercial inverted microscope (IX83, Olympus). The microscope is equipped with a 40 × 0.75NA objective lens and a high-speed sCMOS camera. The illumination part for IDT imaging includes a 195 mm diameter annular LED (containing 28 surface-mounted LEDs) as a light source, positioned 86 mm from the sample, which can achieve matched illumination with NA of 0.75. Each LED operates at ≈200 mW, providing spatially coherent and quasi-monochromatic illumination at a wavelength of 517nm with an FWHM bandwidth of 26 nm. An Field Programmable Gate Array (FPGA) controller manages the sequential activation of the LED elements. The light then passes through the sample, objective lens, and tube lens, being captured by the camera sensor as an intensity image. In the IDT module, 28 intensity images under different LED illumination are sequentially acquired at the focal plane position to reconstruct the 3D RI information of the sample. The FPGA controller coordinates the synchronization between the annular LED and the camera, which is achieved by a pair of coaxial cables that initiate and monitor the exposure status, allowing for the acquisition of intensity datasets from the camera at a rate of 212 Hz (ROI mode, 1024 × 1024 pixels). The fluorescence module is based on the wide-field fluorescence module of the Olympus IX83 inverted microscope, which is equipped with an excitation wavelength of 561nm and a dichroic mirror of 575nm (Semrock, USA) to achieve efficient fluorescence excitation and emission separation. Combined with the electric axis scanning function of the objective lens, we can obtain 3D fluorescence intensity stacks. The experimental system, developed with a C++ program, integrates the camera and microscope Software Development Kit (SDK) development packages and serial communication with the FPGA controller, enabling the control of various components of the imaging system and the automated acquisition of dual-modality images. The detailed process of time-synchronization of hardware components in AO-FIDT image acquisition is presented in Section S3 (Supporting Information).

3. Results and Discussion

3.1. Dynamic 3D RI Imaging of Live HeLa Cells

Conducting dual-modality observations of dynamic cellular motion over tens of hours is a challenging biomedical application for traditional microscopy. Thermal fluctuations in the environment and mechanical instability of the axial scanning system can lead to time-varying aberration and focus drift over time. Although

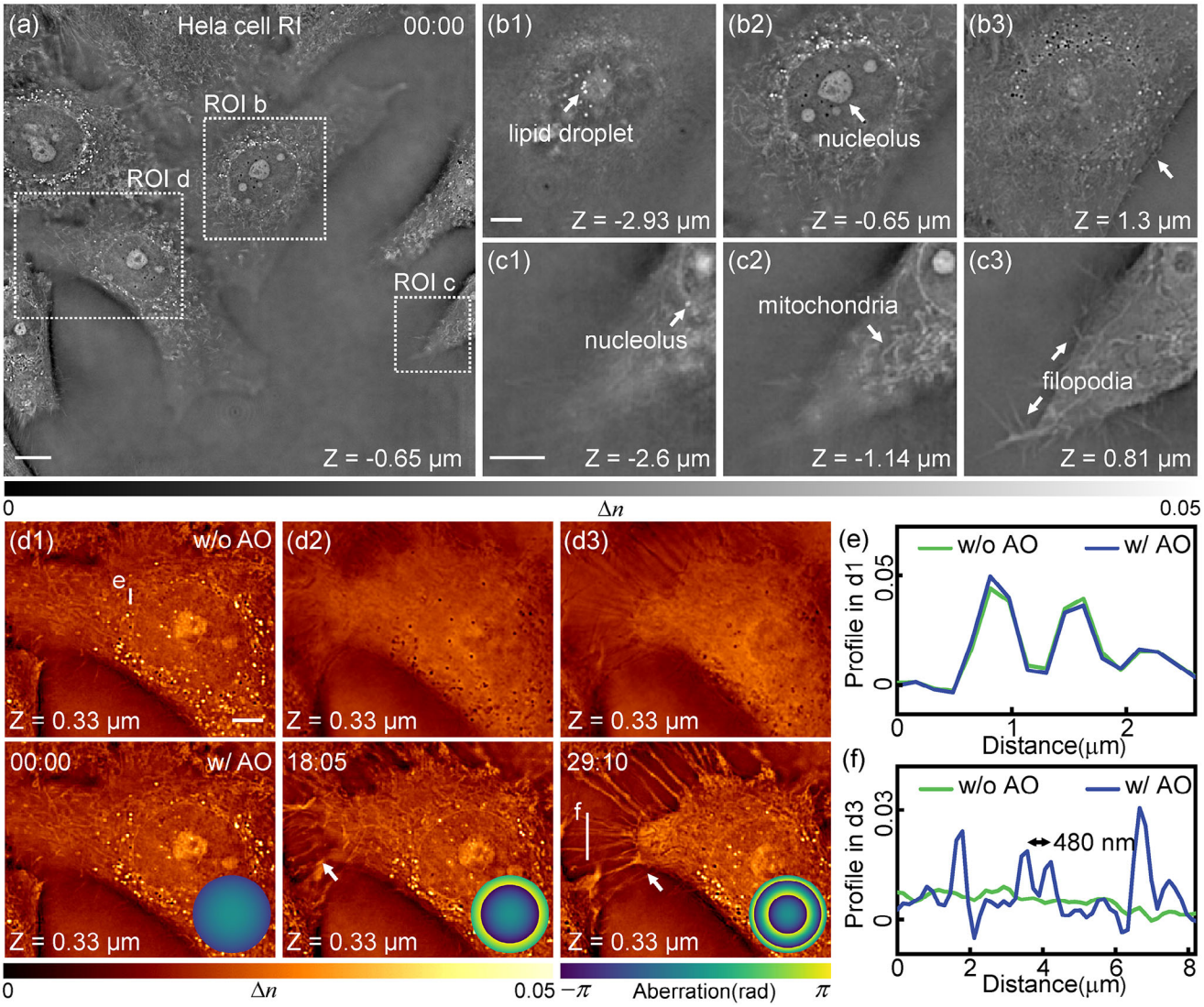

Figure 2. Label-free 3D visualization of the complete apoptosis process of HeLa cells, in which various subcellular structures are observed. a) Full-field RI slice of HeLa cells located at z = -0.65 μm are recovered by AO-FIDT at 00:00, with three different ROI regions magnified within the field of view. The complete visualization process of HeLa cells is provided in Video S1 (Supporting Information). b1–b3, c1–c3) correspond to the (a) subregion, where subcellular structures such as lipid droplets, nucleolus, mitochondria, and filopodia are observed. d1–d3) Comparison of RI slice results without and with AO-assisted during the process of cell apoptosis. Focus drift seriously interferes with the long-term tracking and observation of subcellular organelles. The AO-assisted method can eliminate the time-varying aberrations and achieve long-term stable imaging. e,f) The RI curve across subcellular structures quantified the lateral resolution and RI values. Scale bar, (a) 10 μm; (b, c, d) 5 μm.

the traditional distinction between the focal plane and the defocused plane has become blurred in 3D imaging, information on key layers after focus drift can still be obtained in 3D volume results. However, focus drifts significantly interfere with the long-term tracking and observation of subcellular organelles and pose a challenge to precise axial colocalization in dual-modality imaging. To demonstrate the effectiveness and necessity of our method, we simulated imaging scenarios with environmental thermal fluctuations and applied AO-assisted methods to correct the focus drift caused by time-varying aberrations. HeLa live cells were removed from the incubator and placed on the microscope stage. Within 30 min, the temperature of the cell culture medium gradually decreased from 37.5 °C to the ambient temperature of 26 °C, leading to cell apoptosis. **Figure** 2a illustrates the entire field of view RI slice reconstructed at $z = -0.65$ μm for HeLa cells. Figure 2b,c displays $x - y$ slices at different axial depths at 00:00, showcasing high-resolution visualization of subcellular structures such as mitochondria, cell boundaries, lipid droplets, and filopodia (indicated by white arrows).

Figure 2d compares the dynamic apoptosis process of HeLa cells without and with AO-assisted reconstruction of the RI results. Without AO-assisted, the cellular information characterized at the same z-plane varies significantly at different times, primarily due to focus drift caused by time-varying defocus aberration. With AO-assisted, it is clear that at t = 18:05, the cell exhibits noticeable contraction, with filopodia moving toward

the center and a significant increase in RI contrast (Figure 2 d2, indicated by an arrow). At t = 29:10, the cell rounded up, and the overall morphology of the filopodia adhered to the glass substrate, while some filopodia tips remained attached to their original positions. The contour plots in Figure 2e,f verifies that the AO-FIDT method significantly enhances the stability of the reconstructed RI distribution along the z-axis while ensuring near-diffraction-limited lateral resolution. Additionally, in Video S1 (Supporting Information), we present dynamic imaging data of apoptotic HeLa cells, both with and without the application of AO-assisted.

3.2. Dual-Modality 3D Imaging of Live COS-7 Cells

The AO-FIDT method leverages the strengths of diffraction tomography and fluorescence imaging, offering label-free 3D RI distribution, exceptional spatiotemporal resolution, and the ability to image with high molecular specificity. To demonstrate the combined advantages and practical utility of the proposed method, we conducted a tomographic fluorescence colocalization experiment with COS-7 cells. In the experiment, COS-7 live cells were labeled with MitoTracker Red dye to mark their mitochondria. It is important to note that when measuring live samples, appropriate illumination schemes and exposure times must be chosen to reduce motion-related artifacts. Thanks to the high-speed sCMOS camera used in this experiment, the 28 frames required for each RI reconstruction can be captured with an exposure interval of 5 ms. Thus, the time resolution for label-free imaging per 3D frame is ≈0.14 s. Considering the sample thickness of COS-7 cells, the distribution of mitochondria, and the Nyquist sampling rate, we set the axial fluorescence intensity stack scanning interval to 0.65 μm, with 29 layers in the axial direction. Therefore, the time resolution for fluorescence imaging per 3D frame is ≈5 s. To better capture the movement trajectory of mitochondria and observe the morphological changes of mitochondria after phototoxicity and photobleaching in the fluorescence mode, we performed 3D dual-modality co-localization imaging of the cells at intervals of 20 s. **Figure 3**a displays the full-field deconvoluted fluorescence slice located in the focal plane at the starting time point. Figure 3b,c correspondes to the sub-regions in (a), respectively showing the RI, fluorescence, and dual-modality merged results of COS-7 cells. The RI results show that worm-like, bent, and twisted segments are confirmed to be mitochondria because they perfectly overlap with the structures labeled by the mitochondrial-specific marker MitoTracker Red. The RI result images also provide a global map of the cellular environment and landscape, such as subcellular structures like the nucleus, lipid droplets, and cell membranes.

However, using fluorescence microscopy in conjunction with ODT microscopy is nontrivial. 3D fluorescence imaging requires intense illumination for excitation, which can lead to extensive photobleaching and phototoxicity, adversely affecting cell viability and compromising data integrity. At the same time, the morphology of mitochondria under stress and phototoxic stimulation is a pivotal area of study within the disciplines of metabolism and cell biology, and it is related to numerous clinical pathologies. Therefore, we present in Figure 3d the dual-modality imaging results over 20 min, corresponding to the ROI b area in Figure 3a. The "sphericity" of mitochondria is an essential parameter for assessing phototoxic damage to mitochondria.[35,36] In healthy cells, mitochondria form a tubular morphology (mitos being Greek for "thread"), as shown in Figure 3 d1. Figure 3 d2–d4 observed a progressive sphericity due to light solid excitation, accompanied by mitochondrial fragmentation (white arrows in Figure 3 d2). The white arrows in the RI structure of Figure 3 d3 demonstrate the rapid swelling of mitochondria, deformation, and abruption of inner-membrane cristae, which leads to round, hollow mitochondria.[37] The photobleaching results in Figure 3 d4 indicate that phototoxicity and photobleaching in fluorescence imaging are separate processes, with phototoxicity possibly happening before there is a noticeable reduction in the quality of the imaging. It is demonstrated that the AO-FIDT method is expected to become an important tool in the analysis of subcellular organelle structure and function and in the development of fluorescent dyes.

The AO-FIDT method is also suitable for continuously observing dynamic cellular activities over tens of hours, particularly for detecting cellular structures and dynamics in processes susceptible to phototoxicity, such as mitosis. Figure 4 presents 20 h long-term dual-modality results of COS-7 mitosis. The mitochondria of COS-7 living cells are also labeled with MitoTracker Red dye. **Figure 4**a shows the full-field RI slice of COS-7 cells at the focal plane at time t = 0. Figure 4b,c displays $x-y$ slices at different axial depths at 00:00, demonstrating high-resolution visualization of subcellular structures such as the nucleus, lipid droplets, and mitochondria (indicated by white arrows). To avoid the impact of photobleaching and phototoxicity on cell viability, we used the same image acquisition settings as in Figure 3. Then we performed 3D dual-modality colocalization imaging on the cells in 1 h intervals. Figure 4d shows the dual-modality results of the COS-7 cell division process. Due to environmental thermal fluctuations and mechanical instability caused by the axial acquisition of fluorescence images, there is a noticeable change in the time-varying aberrations of the imaging system, and the corresponding corrected solution varies significantly throughout the imaging process. Figure 4d demonstrates the capability of the AO-FIDT method to track organelle motion and cellular morphological changes over long timescales, enabling precise colocalization of the refractive index and fluorescence results along the axial direction in 3D dynamic imaging.

Compared to the sensitivity of mitochondria to excessive phototoxicity from labeled fluorescent indicators during imaging, label-free 3D RI imaging does not cause photobleaching or phototoxicity, as demonstrated by continuous 3D RI imaging of cells without disrupting the division process. Figure 4e shows the results of the continuous detection of mitochondria in COS-7 live cells, corresponding to the sub-region ROI e in Figure 4a. It is found that mitochondria may actively transform their shape, position, and possible functions based on the cell statement. At t = 00:01, the cell is in a slow-motion state, and under low energy demand, mitochondria adopt a tubular shape to increase metabolic efficiency. As the cell begins to divide, mitochondria become shorter and rounder, moving toward the position of the cell nucleus to meet the increased energy demand. The experimental results show that AO-assisted label-free 3D RI imaging can perform full-field, high spatiotemporal resolution, and indefinite imaging of cells, providing continuous information on

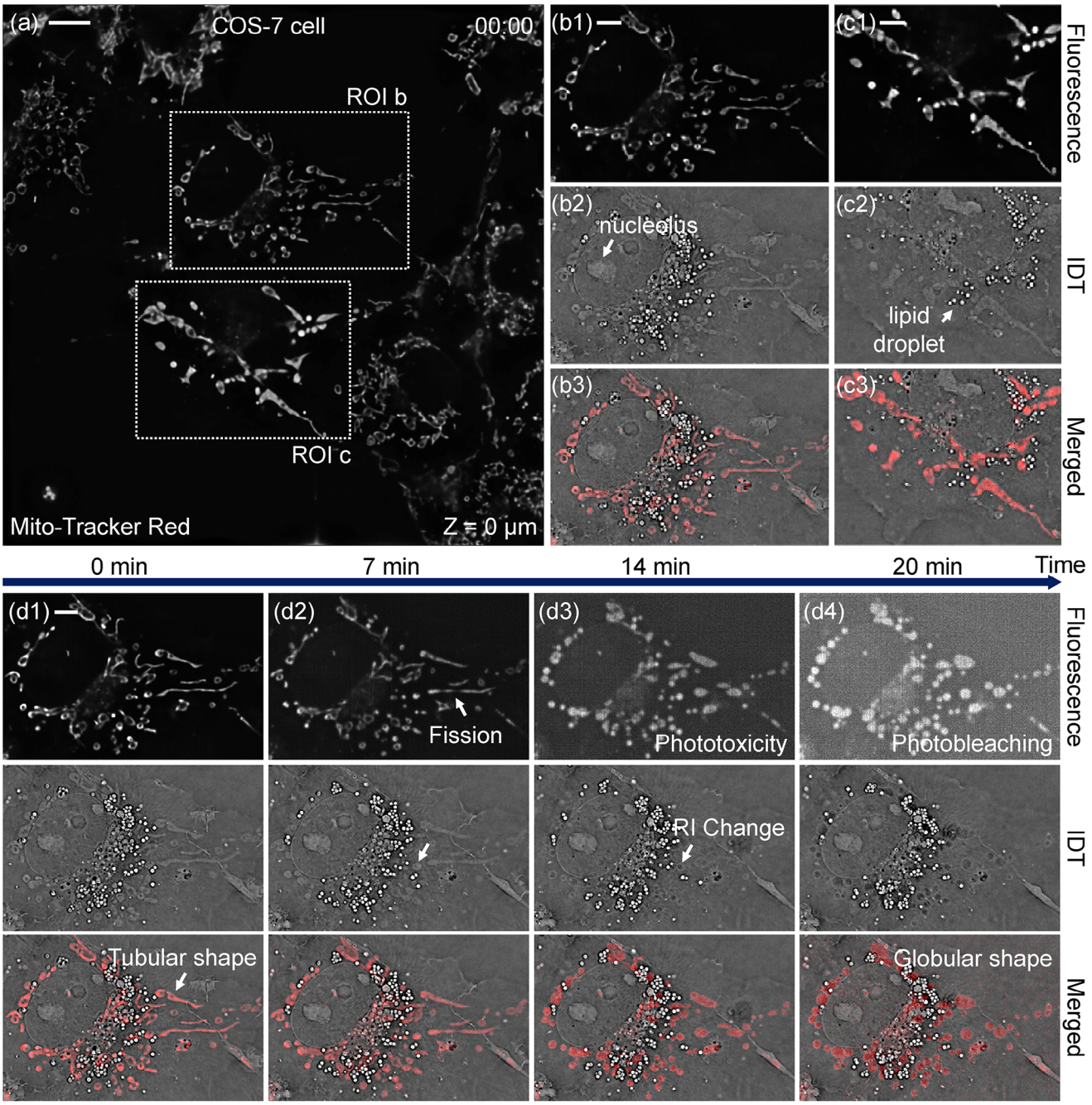

Figure 3. COS-7 live cells were stained with MitoTracker Red dye for mitochondria, and then the dynamic imaging results of 3D dual-modality were obtained by the AO-FIDT method. a) Full-field fluorescence slice of COS-7 cells located in the focal plane at the starting time. b1–b3,c1–c3) The fluorescence, RI, and dual-modality merge results were restored by AO-FIDT, corresponding to the subregion in (a), respectively. Label-free RI imaging can optically detect subcellular organelles such as lipid droplets, nucleolus, and cell Membranes. Fluorescence imaging can observe high-contrast views of mitochondria. d1–d4) Dual-modality time-lapse imaging results of 20 min for the sub-region ROI b in (a), where the mitochondria, affected by phototoxicity, change from tubular to spherical. Scale bars, (a) 10 μm; (b, c, d) 5 μm.

long-term cellular processes and enabling the visualization of rare structures and intermediates. Combined with 3D fluorescence organelle labeling, it can clarify the identity of subcellular structures under different spatiotemporal dynamics, accelerating scientific discoveries.

4. Conclusion

To conclude, we proposed a novel AO-FIDT method and constructed the corresponding experimental setup. This new approach integrates AO-assisted aberration correction with IDT

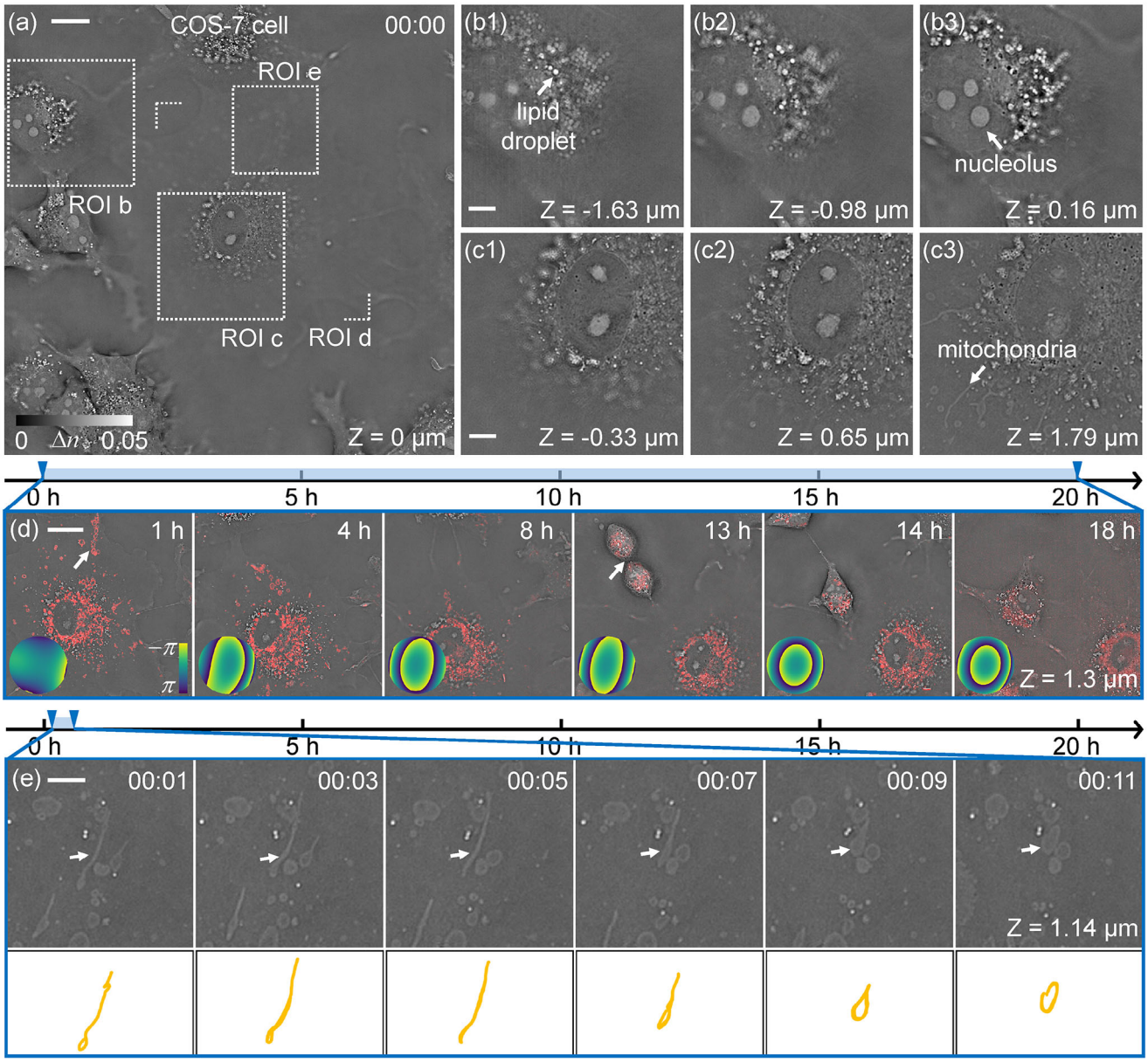

Figure 4. Time-lapse dual-modality imaging of the mitotic process in COS-7 cells using the AO-FIDT method. a) Full-field RI slice of COS-7 cells located in the focal plane at the starting time. b1–b3,c1–c3) RI slices restored by AO-FIDT correspond to the sub-regions in (a), where subcellular structures such as lipid droplets, the nucleus, and mitochondria are observed. d) Dual-modality imaging results of the COS-7 cell division process, in which adaptive optics assistance effectively locks the focal plane, enabling long-term tracking of organelles and precise colocalization of refractive index and fluorescence along the axial direction. The entire visualization of COS-7 cell division is detailed in Video S2 (Supporting Information). e) High spatiotemporal resolution imaging results of mitochondria. Scale bars, (a) 25 μm; (d) 20 μm; (b, c, e) 5 μm.

modality and uniquely employs an iterative ptychographic approach to effectively separate the coupled 3D RI and aberrations from the captured unlabeled intensity images. Meanwhile, we provided feedback on the real-time calculated aberrations solution to the point spread function of the system to synchronously correct the 3D fluorescence results, thereby significantly enhancing the reconstruction quality of the fluorescence modality. Reconstruction results on live HeLa cells demonstrate that the proposed AO-FIDT method can effectively overcome focus drift caused by time-varying aberrations and mechanical errors without compromising speed and resolution, thereby enhancing the imaging performance for long-term research, such as live cell observations. Additionally, non-interferometry diffraction tomography can comprehensively display the interactions of organelles within live cells in 3D without the need for additional labeling and complex experiment setup. Combined with the fluorescence imaging modality, the standard for molecular-specific visualization, AO-FIDT emerges as an effective imaging solution that enables comprehensive and synergistic analysis of biological components/interactions previously only researched

in isolation. Long-term dual-modality imaging results from COS-7 cells indicate that the proposed AO-FIDT can image the morphology and characteristics of subcellular organelles, such as mitochondria, with high spatiotemporal resolution. As far as we are aware, this marks the initial instance in which AO-assisted technology has been applied to 3D dual-modality imaging, achieving long-term, high spatiotemporal resolution 3D dual-modality cell imaging results. This breakthrough highlights the potential of AO-FIDT as a leading non-invasive technology for probing the structure and dynamics of biological phenomena at the cellular and subcellular scales.

Nonetheless, several key issues warrant further exploration or clarification. First, the AO-FIDT method we propose uses label-free IDT to provide a comprehensive 3D view of the cellular. However, its theoretical framework continues to depend on the first-order Rytov approximation. The validity of this model is contingent upon the RI within the sample, which may restrict its use in samples that exhibit multiple layers or significant scattering.[38–41] Second, although the AO-FIDT method can serve as an important tool for bioanalysis, diffraction still limits its imaging resolution. Meanwhile, 3D volumetric fluorescence requires strong illumination to excite the sample, leading to extensive photobleaching and phototoxicity. The mechanical speed variation of the axial focal plane also constrains the temporal resolution. In our future work, we could consider integrating fluorescence super-resolution techniques (such as SIM) into AO-FIDT.[12,13,42,43] By leveraging the super-resolution capabilities of SIM, additional biomolecular specificity can be achieved, such as internal structural information of subcellular organelles like mitochondrial cristae. This dual-modality synergy strategy can avoid the limitations of existing 3D fluorescence methods, providing a new avenue for a more comprehensive exploration of cellular and subcellular dynamics, and is expected to significantly advance the field of biological imaging.

Supporting Information

Supporting Information is available from the Wiley Online Library or from the author.

Acknowledgements

N.Zhou, R.Zhang, and R.Zhu contributed equally to this work. This work was supported by the National Natural Science Foundation of China (62227818, 62361136588, 62105156, 62305162, U21B2033), National Key Research and Development Program of China (2022YFA1205002, 2024YFE0101300, 2024YFF0505603, 2024YFF0505600), Biomedical Competition Foundation of Jiangsu Province (BE2022847), Key National Industrial Technology Cooperation Foundation of Jiangsu Province (BZ2022039), Fundamental Research Funds for the Central Universities (30923010206, 2023102001, 2024202002), National Key Laboratory of Plasma Physics (JCKYS2024212804), and Open Research Fund of Jiangsu Key Laboratory of Spectral Imaging & Intelligent Sense (JSGP202105, JSGP202201, JSGPCXZNGZ202401).

Conflict of Interest

The authors declare no conflict of interest.

Data Availability Statement

The data that support the findings of this study are available from the corresponding author upon reasonable request.

Keywords

3D microscopy, adaptive optics, dual-modality imaging, fourier ptychographic diffraction tomography

Received: December 15, 2024
Revised: February 2, 2025
Published online:

[1] E. M. Christiansen, S. J. Yang, D. M. Ando, A. Javaherian, G. Skibinski, S. Lipnick, E. Mount, A. O'neil, K. Shah, A. K. Lee, P. Goyal, W. Fedus, R. Poplin, A. Esteva, M. Berndl, L. L. Rubin, P. Nelson, S. Finkbeiner, *Cell* **2018**, *173*, 792.
[2] J. G. McNally, T. Karpova, J. Cooper, J. A. Conchello, *Methods* **1999**, *19*, 373.
[3] A. Mermillod-Blondin, E. McLeod, C. B. Arnold, *Opt. Lett.* **2008**, *33*, 2146.
[4] S. Shin, D. Kim, K. Kim, Y. Park, *Sci. Rep.* **2018**, *8*, 9183.
[5] X. Huang, J. Fan, L. Li, H. Liu, R. Wu, Y. Wu, L. Wei, H. Mao, A. Lal, P. Xi, L. Tang, Y. Zhang, Y. Liu, S. Tan, L. Chen, *Nat. Biotechnol.* **2018**, *36*, 451.
[6] C. Ounkomol, S. Seshamani, M. M. Maleckar, F. Collman, G. R. Johnson, *Nat. Methods* **2018**, *15*, 917.
[7] E. Wolf, *Opt. Commun.* **1969**, *1*, 153.
[8] Y. Sung, W. Choi, C. Fang-Yen, K. Badizadegan, R. R. Dasari, M. S. Feld, *Opt. Express* **2009**, *17*, 266.
[9] N. Zhou, R. Zhang, W. Xu, R. Zhu, H. Tang, X. Zhou, J. Sun, P. Gao, Q. Chen, C. Zuo, *Laser Photonics Rev.* **2024**, 2400387.
[10] N. Zhou, J. Li, J. Sun, R. Zhang, Z. Bai, S. Zhou, Q. Chen, C. Zuo, *Opt. Lett.* **2022**, *47*, 969.
[11] K. Kim, W. S. Park, S. Na, S. Kim, T. Kim, W. Do Heo, Y. Park, *Biomed. Opt. Express* **2017**, *8*, 5688.
[12] D. Dong, X. Huang, L. Li, H. Mao, Y. Mo, G. Zhang, Z. Zhang, J. Shen, W. Liu, Z. Wu, G. Liu, Y. Liu, H. Yang, Q. Gong, K. Shi, L. Chen, *Light: Sci. Appl.* **2020**, *9*, 11.
[13] S. Chowdhury, W. J. Eldridge, A. Wax, J. A. Izatt, *Biomed. Opt. Express* **2017**, *8*, 5776.
[14] Z. Cai, R. Zhang, N. Zhou, Q. Chen, C. Zuo, *Laser Photonics Rev.* **2023**, *17*, 2300217.
[15] R. Zhang, N. Zhou, H. Tang, M. Xia, Z. Cai, J. Sun, Q. Chen, C. Zuo, *Laser Photonics Rev.* **2024**, *18*, 2300770.
[16] N. Komatsu, Y. Fujita, M. Matsuda, K. Aoki, *Oncogene* **2015**, *34*, 5607.
[17] P. Song, S. Jiang, H. Zhang, X. Huang, Y. Zhang, G. Zheng, *APL Photonics* **2019**, *4*, 050802.
[18] X. Ou, G. Zheng, C. Yang, *Opt. Express* **2014**, *22*, 4960.
[19] W. Wang, Z. Huang, *Opto-Electron. Adv.* **2024**, *7*, 240064.
[20] Y. Shu, J. Sun, J. Lyu, Y. Fan, N. Zhou, R. Ye, G. Zheng, Q. Chen, C. Zuo, *PhotoniX* **2022**, *3*, 24.
[21] L. Lu, J. Li, Y. Shu, J. Sun, J. Zhou, E. Y. Lam, Q. Chen, C. Zuo, *Adv. Photonics* **2022**, *4*, 056002.
[22] R. Horstmeyer, J. Chung, X. Ou, G. Zheng, C. Yang, *Optica* **2016**, *3*, 827.
[23] C. Zuo, J. Sun, J. Li, A. Asundi, Q. Chen, *Opt. Lasers Eng.* **2020**, *128*, 106003.
[24] N. Zhou, J. Sun, R. Zhang, R. Ye, J. Li, Z. Bai, S. Zhou, Q. Chen, C. Zuo, *ACS Photonics* **2023**, *10*, 2461.
[25] P. Sarder, A. Nehorai, *IEEE Signal Process Mag.* **2006**, *23*, 32.

[26] D. S. Biggs, *Curr. Protoc. Cytom.* **2010**, *52*, 12.
[27] S. Zhou, J. Li, J. Sun, N. Zhou, H. Ullah, Z. Bai, Q. Chen, C. Zuo, *Optica* **2022**, *9*, 1362.
[28] J. Li, N. Zhou, Z. Bai, S. Zhou, Q. Chen, C. Zuo, *Opt. Lasers Eng.* **2021**, *143*, 106624.
[29] C. Zuo, J. Sun, Q. Chen, *Opt. Express* **2016**, *24*, 20724.
[30] M. Lee, K. Kim, J. Oh, Y. Park, *Light: Sci. Appl.* **2021**, *10*, 102.
[31] J. Lim, K. Lee, K. H. Jin, S. Shin, S. Lee, Y. Park, J. C. Ye, *Opt. Express* **2015**, *23*, 16933.
[32] L. B. Lucy, *Astronom. J.* **1974**, *79*, 745.
[33] W. H. Richardson, *JoSA* **1972**, *62*, 55.
[34] N. Dey, L. Blanc-Feraud, C. Zimmer, P. Roux, Z. Kam, J.-C. Olivo-Marin, J. Zerubia, *Microsc. Res. Tech.* **2006**, *69*, 260.
[35] R. I. K. Geltink, D. O'Sullivan, M. Corrado, A. Bremser, M. D. Buck, J. M. Buescher, E. Firat, X. Zhu, G. Niedermann, G. Caputa, B. Kelly, U. Warthorst, A. Rensing-Ehl, R. L. Kyle, L. Vandersarren, J. D. Curtis, A. E. Patterson, S. Lawless, K. Grzes, J. Qiu, D. E. Sanin, O. Kretz, T. B. Huber, S. Janssens, B. N. Lambrecht, A. S. Rambold, E. J. Pearce, E. L. Pearce, *Cell* **2017**, *171*, 385.
[36] A. Bahat, A. Goldman, Y. Zaltsman, D. H. Khan, C. Halperin, E. Amzallag, V. Krupalnik, M. Mullokandov, A. Silberman, A. Erez, A. D. Schimmer, J. H. Hanna, A. Gross, *Nat. Commun.* **2018**, *9*, 5132.
[37] Z. Yang, L. Li, J. Ling, T. Liu, X. Huang, Y. Ying, Y. Zhao, Y. Zhao, K. Lei, L. Chen, Z. Chen, *Chem. Sci.* **2020**, *11*, 8506.
[38] J. Zhu, H. Wang, L. Tian, *Opt. Express* **2022**, *30*, 32808.
[39] M. Chen, D. Ren, H.-Y. Liu, S. Chowdhury, L. Waller, *Optica* **2020**, *7*, 394.
[40] R. Wang, L. Yang, Y. Lee, K. Sun, K. Shen, Q. Zhao, T. Wang, X. Zhang, J. Liu, P. Song, et al., *Adv. Opt. Mater.* **2024**, 2303028.
[41] S. Jiang, C. Guo, T. Wang, J. Liu, P. Song, T. Zhang, R. Wang, B. Feng, G. Zheng, *ACS Sens.* **2022**, *7*, 1058.
[42] K. Wen, X. Fang, Y. Ma, M. Liu, S. An, J. Zheng, T. Kozacki, P. Gao, *Opt. Lett.* **2022**, *47*, 2666.
[43] J. Qian, Y. Cao, Y. Bi, H. Wu, Y. Liu, Q. Chen, C. Zuo, *eLight* **2023**, *3*, 4.